Response of the San Andreas fault to the 1983 Coalinga-Nuñez earthquakes: An application of interaction-based probabilities for Parkfield

Shinji Toda

Active Fault Research Center, Geological Survey of Japan, National Institute of Advanced Industrial Science and Technology, Tsukuba, Japan

Ross S. Stein

U.S. Geological Survey, Menlo Park, California, USA

Received 22 January 2001; revised 17 December 2001; accepted 22 December 2001; published 29 June 2002.

[1] The Parkfield-Cholame section of the San Andreas fault, site of an unfulfilled earthquake forecast in 1985, is the best monitored section of the world's most closely watched fault. In 1983, the M = 6.5 Coalinga and M = 6.0 Nuñez events struck 25 km northeast of Parkfield. Seismicity rates climbed for 18 months along the creeping section of the San Andreas north of Parkfield and dropped for 6 years along the locked section to the south. Right-lateral creep also slowed or reversed from Parkfield south. Here we calculate that the Coalinga sequence increased the shear and Coulomb stress on the creeping section, causing the rate of small shocks to rise until the added stress was shed by additional slip. However, the 1983 events decreased the shear and Coulomb stress on the Parkfield segment, causing surface creep and seismicity rates to drop. We use these observations to cast the likelihood of a Parkfield earthquake into an interaction-based probability, which includes both the renewal of stress following the 1966 Parkfield earthquake and the stress transfer from the 1983 Coalinga events. We calculate that the 1983 shocks dropped the 10-year probability of a $M \sim 6$ Parkfield earthquake by 22% (from 54 ± 22% to 42 ± 23%) and that the probability did not recover until about 1991, when seismicity and creep resumed. Our analysis may thus explain why the Parkfield earthquake did not strike in the 1980s, but not why it was absent in the 1990s. We calculate a 58 ± 17% probability of a $M \sim 6$ Parkfield earthquake during 2001–2011. *INDEX TERMS:* 7223 Seismology: Seismic hazard assessment and prediction; 7230 Seismology: Seismicity and seismotectonics; 7260 Seismology: Theory and modeling; *KEYWORDS:* Coalinga earthquake, Parkfield, stress change, earthquake probability, seismicity rate

1. Introduction

[2] Recent efforts to explain earthquake interaction by stress transfer have drawn support from the association between Coulomb stress changes and seismicity rate changes [*Reasenberg and Simpson*, 1992; *Toda et al.*, 1998; *Stein*, 1999; *Wyss and Wiemer*, 2000]. Stress increases are seen to be followed by increases in seismicity rate followed by a decay toward the background rate. Although seismicity rate increases are readily detectable, measurement of decreases is best achieved on the rare faults with very high rates of background seismicity. Probability models incorporating earthquake interaction by stress transfer [*Dieterich and Kilgore*, 1996; *Parsons et al.*, 2000] suffer from the need to average stress changes and constitutive parameters over fault surfaces much larger than the site of earthquake nucleation. Study of the Coalinga-Parkfield interaction helps to overcome these obstacles: First, the creeping section has among the highest rates of microearthquakes of any fault in the United States, making detection of seismicity rate decreases much easier [*Miller*, 1996; *Poley et al.*, 1987; *Wiemer and Wyss*, 1997; *Wyss et al.*, 1990] (Figure 1b). Second, the 1983 events were large enough to impart significant stress to the San Andreas, but far enough away that the unknown details of the 1983 fault slip have a negligible impact on the stress transfer (Figure 1a). Third, synthesis of the rich assemblage of seismic, geodetic, and surface creep data at Parkfield permits an assessment of the parameters needed for an interaction probability analysis. Finally, the 1934 and 1966 Parkfield shocks nucleated within a 5 × 5 km fault patch [*Bakun and McEvilly*, 1979, 1984], and the earthquake slip in 1934 and 1966 was similar north of Cholame [*Segall and Du*, 1993], so one can focus on the site of past, and perhaps future, earthquake nucleation and rupture.

0148-0227/02/2001JB000172$09.00

2. Calculation of Seismicity Rate Change

[3] Seismicity within a 120-km-long by 10-km-wide rectangle aligned with the San Andreas fault with endpoints at 36.50°N, 121.08°W; 35.66°N, 120.20°W was

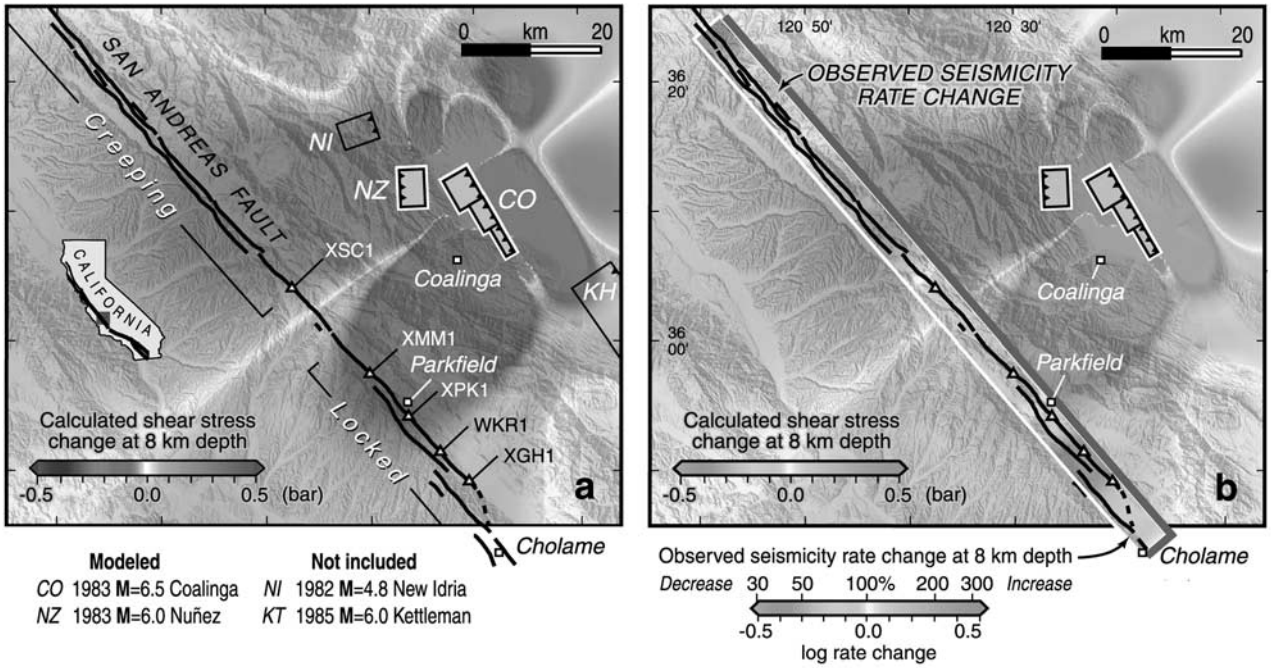

Figure 1. (a) Shear stress transferred by the 2 May 1983 $M = 6.5$ Coalinga (CO) and 11 June to 22 July $M = 6.0$ Nuñez (NZ) earthquakes on vertical right-lateral planes parallel to the San Andreas fault at 8 km depth. Source parameters for CO are from *Stein and Ekström* [1992] for the coseismic period: 150° strike, 15°W dip, 4.7 m reverse slip, 10 km upper depth, and 1.5–4.0 km width; for NZ they are based on work by *Eaton* [1990] and *Rymer et al.* [1990]: 178° strike, 65°E dip, 0.22 m right-lateral and 0.65 m reverse slip, 5.4 km length, and 2 km upper and 8.3 km width. Excluded because of their negligible impact on the stress are the 25 October 1982 $M = 4.8$ New Idria (NI) shock and the 4 August 1985 $M = 6.0$ Kettleman Hills (KH) shock [*Ekström et al.*, 1992]. (b) The observed seismicity rate change is superimposed along the San Andreas fault, also at 8 km depth. Relocated $M = 1.3$ seismicity is from the NCSN in a 10-km-wide box with endpoints at 36.50°/−121.08° 35.65°/−120.20°. See color version of this figure at back of this issue.

extracted from the Northern California Seismic Network (NCSN). $M \geq 1.3$ earthquakes were relocated by F. Waldhauser using the current NCSN Parkfield velocity model and a double-difference algorithm [*Waldhauser et al.*, 1999]. Relocation reduces the errors in depth and in location (Figure 2a), enabling us to examine the seismicity rate change in both map view and cross section. The cumulative number of $M = 1.3$ earthquakes as a function of time is shown in Figure 2b; relocation introduces no obvious temporal artifacts, and only 4% of the earthquakes could not be relocated. We measure the seismicity rate starting from May 1980 because a shift in U.S. Geological Survey (USGS) magnitudes relative to University of California, Berkeley, magnitudes occurred in 1978–1980 [*Wiemer and Wyss*, 1997; S. Wiemer, written communication, 2000], which would produce systematic errors in rate calculations before this time.

[4] Unlike the seismic moment rate, the seismicity rate counts earthquakes irrespective of magnitude. Because the smallest included shocks are most abundant, they will be most influential. The minimum magnitude of complete reporting, M_c defines the ideal lower magnitude limit for inclusion in seismicity rate calculations. To determine M_c for 1980–1990, we plot the departure of a power law fit of the frequency-magnitude distribution in Figure 3a, following *Wiemer and Wyss* [2000]. At the 90% confidence level used by *Wiemer and Wyss* [2000], $M_c = 1.3$, a result consistent with the histogram in Figure 3c, which shows that the number of shocks climbs as the magnitude is decreased through 1.3. To guard against systematic errors arising if M_c changed with time, we calculate M_c for the both pre- and post-Coalinga periods in Figure 3b; $M_c = 1.3$ in both cases.

3. Observations of Seismicity Rate Change

[5] The rate of seismicity along the San Andreas fault increased after Coalinga for ~18 months in the creeping zone (Figure 2c), whereas it decreased and remained low for more than 3 years in the locked zone (Figure 2d). The seismicity rate change is plotted as a function of depth in Figure 4. During 1985–1990 the seismicity rate returned roughly to normal along the creeping section but remained low along the Parkfield section (Figure 4e). After 1990 the seismicity rate returned approximately to normal everywhere (Figure 4f). In Figures 1 and 4 the number of earthquakes in cylindrical volumes of 5-km radius with centers spaced 1 km apart is computed for pre- and post-Coalinga periods. The rate change is smoothed with a Gaussian filter for every volume in which there are at least six shocks in total and for which there is at least one pre-Coalinga shock [*Matthews and Reasenberg*, 1988; *Reasen-*

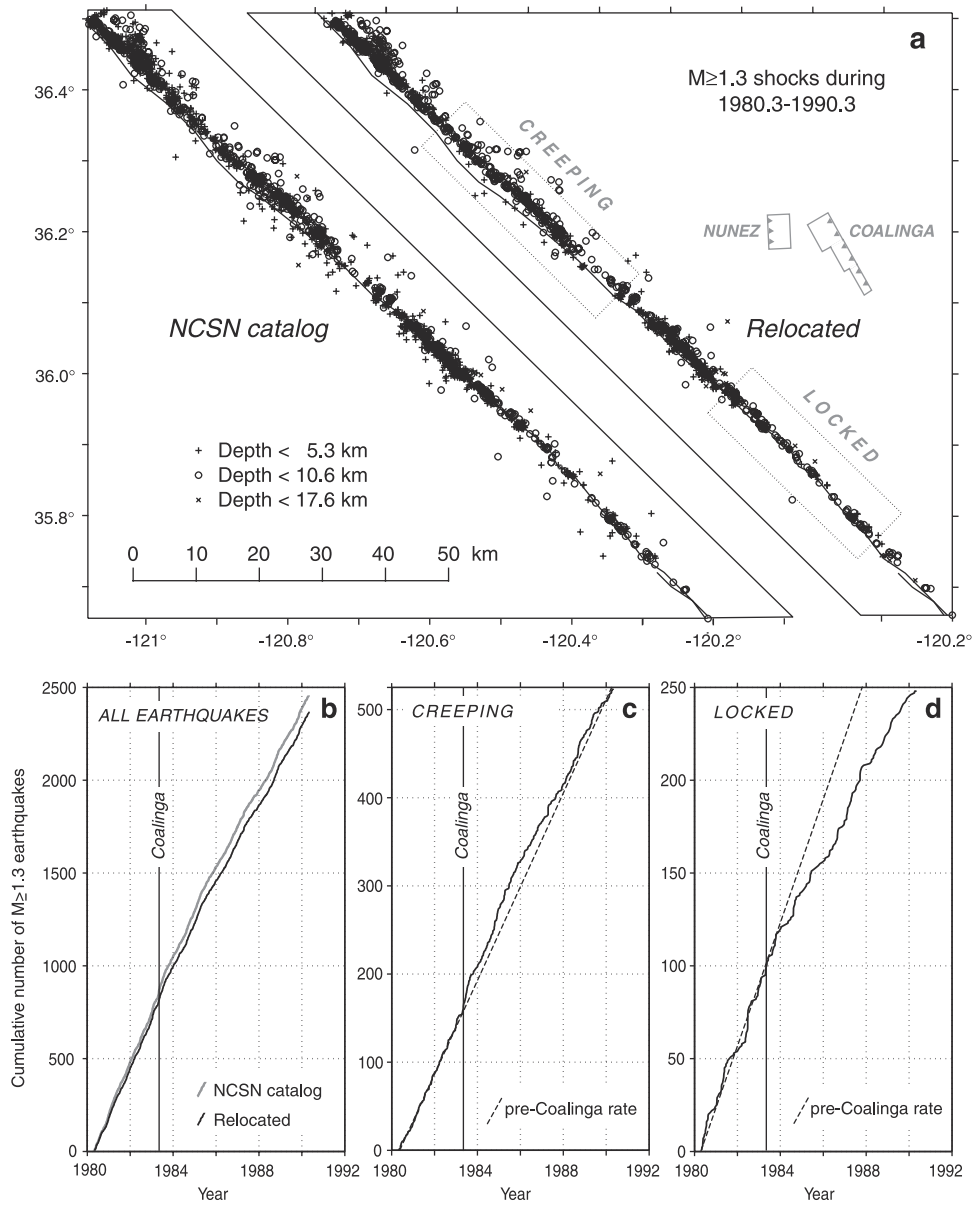

Figure 2. Seismicity along the San Andreas fault in the vicinity of the 1983 Coalinga-Nuñez earthquakes. (a) (left) Northern California Seismic network (NCSN) catalog locations and (right) double-difference relocations following *Waldhauser and Ellsworth* [2000]. Endpoints of the box in the "locked" zone are 35.978°/−120.537° 35.749°/−120.306° width is 10 km; depth is 3–12 km. For the box in the "creeping" zone they are 36.368°–120.934°; 36.096°/−120.657° width is 10 km; depth is 2–10 km. (b) Number of earthquakes as a function of time, which is little different for the NCSN and relocated shocks. (c) Seismicity rate, which is seen to rise for ∼18 months after Coalinga in the creeping section. (d) Drop in the seismicity rate in the 1966 Parkfield rupture zone within several months after the Coalinga shock. Relocated earthquakes are shown in Figures 2c and 2d.

berg and Simpson, 1992]. Because more accurately relocated post-1990 Parkfield seismicity using waveform cross correlation shows few, if any, earthquakes in the uppermost 2 km [*Rubin et al.*, 1999], we regard rate changes in the upper 2 km in the 1980–1990 data as unreliable, and they are not considered.

[6] To test whether the seismicity rate changes are unduly influenced by the Gaussian filter, we also calculated rate changes with just 15% of the smoothing. The same trends are evident but with greater spatial variation. (Both smoothed and unsmoothed observations are carried into the regression analysis in section 4.) To test the significance of the rate changes, we plot the Z statistic of *Habermann* [1983] for several time periods in Figures 5b–5d. These plot the statistical significance of a rate change, rather than the value of the change, relative to expected random errors. The largest seismicity rate changes in Figure 4 correspond to the largest Z values (exceeding ±3) in Figure 5, suggesting that

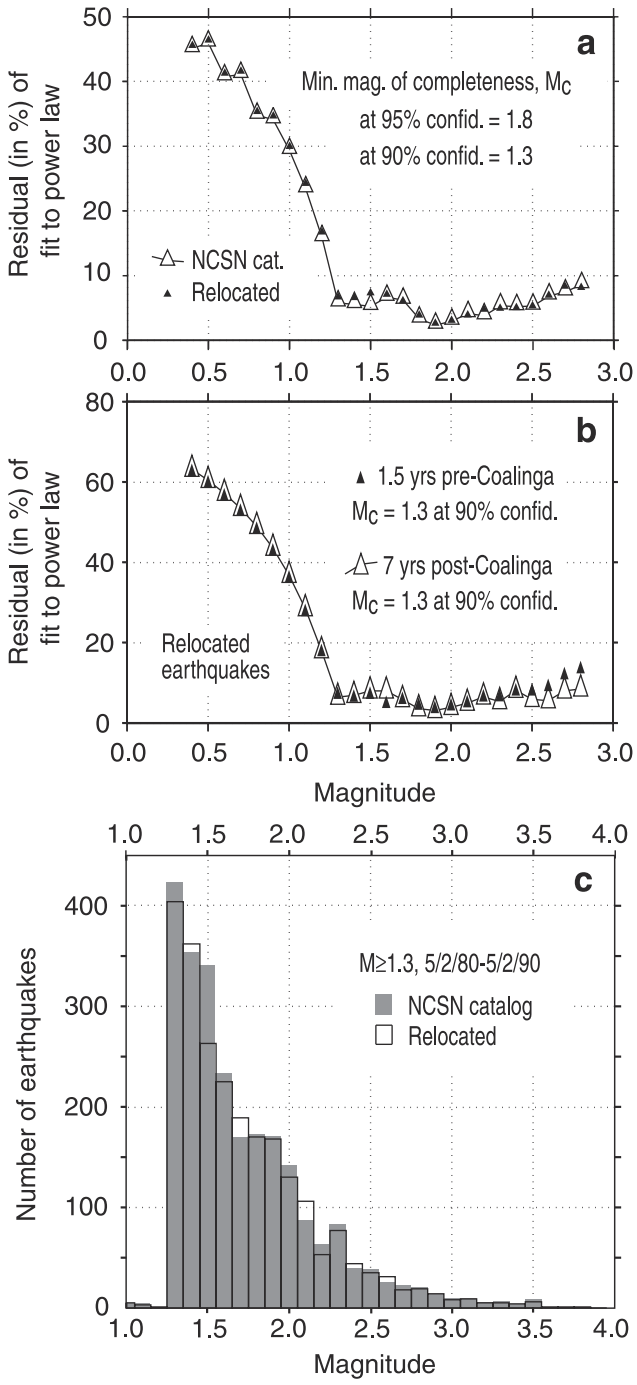

Figure 3. Calculation of the minimum magnitude of complete reporting, M_c, following *Wiemer and Wyss* [2000]. (a) M_c = 1.3 for both the NCSN and relocated earthquakes. (b) M_c = 1.3 for both the 3-year pre-Coalinga and 7-year post-Coalinga periods. (c) Histogram of the number of earthquakes in each magnitude band, the data used to construct Figures 3a and 3b.

except at the southern end of the 1966 Parkfield rupture zone where the lower rate of seismicity precludes calculation of Z, the rate changes are significant. The 5 × 5 km Parkfield hypocentral zone exhibits a Z value of 2.0–2.5 for the longer intervals (Figures 5c and 5d).

4. Correlation of Seismicity and Stress Changes

[7] Several studies [*Parsons et al.*, 1999; *Reasenberg and Simpson*, 1992; *Stein*, 1999; *Toda et al.*, 1998] have found that seismicity rate change is correlated with the calculated Coulomb stress change, ΔCFF

$$\Delta\mathrm{CFF} = \Delta\tau + \mu\Delta\sigma, \quad (1)$$

where τ is the shear stress and σ is the normal stress, positive for unclamping. If correct, not only should aftershocks be more prevalent in regions of Coulomb stress increase, but the rate of earthquakes should drop in regions of stress decrease. The calculated shear stress change on the San Andreas fault imparted by the Coalinga-Nuñez events resembles the observed seismicity rate change along the fault at midcrustal depths in map view (Figure 1b) and in cross section (compare Figures 4b and 4d). This correspondence suggests a causal relationship: San Andreas earthquakes became nearly twice as frequent (a log rate change of +0.3) where the stress increased by ~0.5 bar, and roughly half as frequent (log rate change of −0.3), where the stress decreased by the same amount. That the shear stress rose on the creeping section and dropped on the locked Parkfield-Cholame section (Figure 1) is simply an accident of Coalinga's location; had the 1983 earthquakes struck north or south of Coalinga, the stress distribution in the San Andreas would have differed.

[8] The seismicity rate change and Coulomb stress change are statistically correlated, but the extent to which the correlation is driven by the shear stress change is equivocal. Visual inspection of Figures 2b and 2d suggests the shear stress controls the seismicity rate change (e.g., $\mu \sim 0$ in equation (1)). However, a spatial regression of the Coulomb stress change on seismicity rate change (Figures 6b and 6c) indicates that the regression coefficient, R, increases with μ. A regression plot for $\mu = 0.4$ is shown in Figure 6a. The dependence of the seismicity rate change on stress change (i.e., the slope of the regression), on the other hand, decreases as μ grows from 0.2 to 0.8. Thus, in our judgment, the data lack the sensitivity to suggest more than $0.2 \leq \mu \leq 0.8$. Regardless of the amount of smoothing or the assumed value of friction, the y intercept is about −0.1, suggesting that the seismicity rates are biased toward negative values (i.e., in the absence of a stress change, the seismicity rates appear to decrease after May 1983). The bias is probably an artifact of the magnitude shift in the catalog that was not fully removed by using data starting from May 1980. (Using only later data does not circumvent this problem because the pre-Coalinga period would become too short to adequately measure seismicity rates.)

5. Analysis of Surface Creep Changes

[9] Data from fault creep meters (Figure 1a) permit independent analysis of the Coalinga stress transfer and, together with the seismic data, enable us to gauge parameters for a probability estimate. Surface creep slowed, stopped, or reversed on all creep meters for 1–4 years

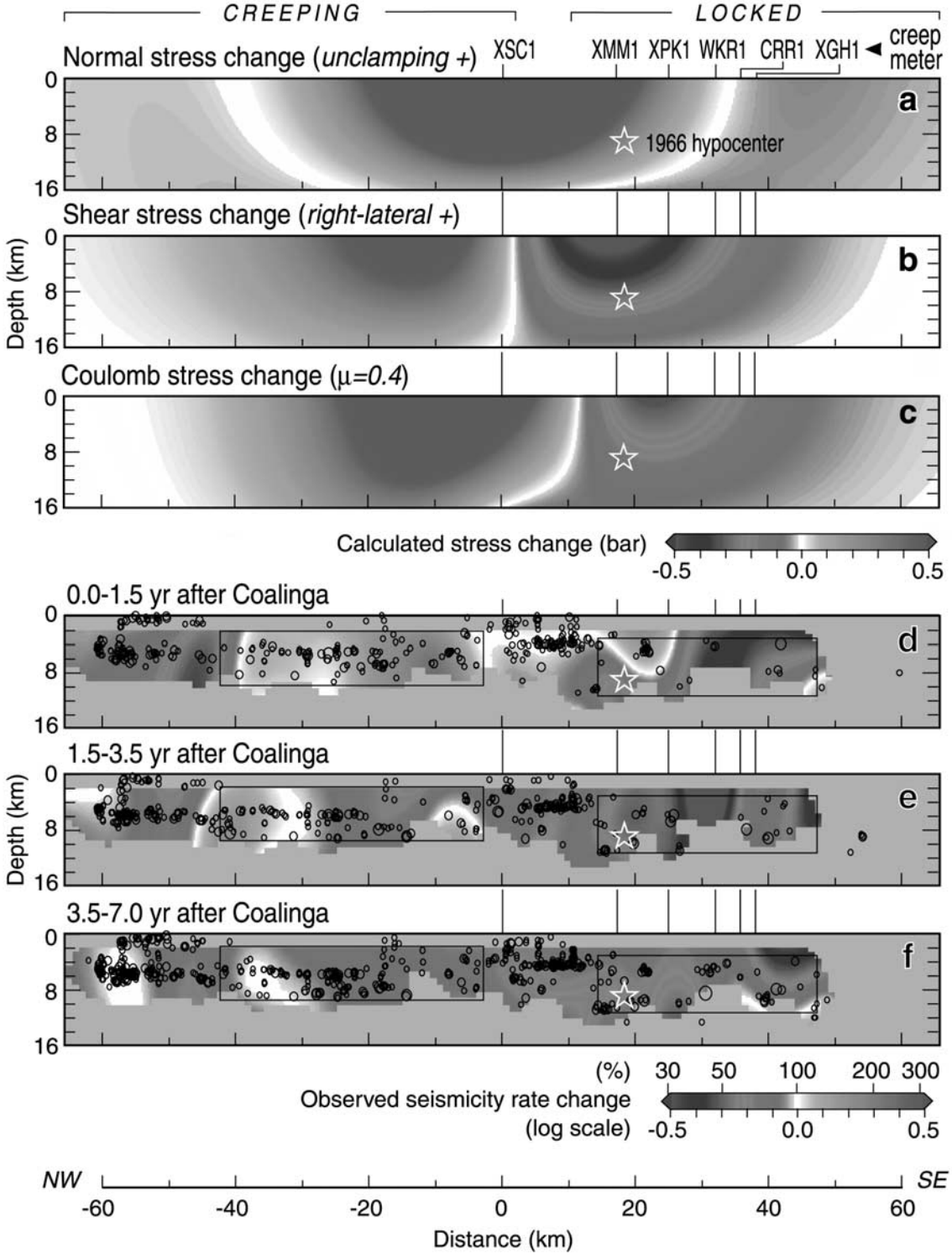

Figure 4. (a) Calculated normal, (b) shear, and (c) Coulomb stress change and (d–f) observed seismicity rate change within 5 km of the San Andreas fault associated with the 1983 Coalinga-Nuñez shocks, with earthquakes during the indicated post-Coalinga period superimposed in black. The seismicity rate change for the post-Coalinga 1.5-year period 2 May 1983 to 1 November 1984 (Figure 4d) and the 5.5-year period 2 November 1984 to 1 May 1990 (Figure 4e) are calculated relative to the 3-year pre-Coalinga period 2 May 1980 to 1 May 1983. The stress changes are similar to those of *Simpson et al.* [1988]. Note the association between the calculated shear stress change (Figure 4b) and the observed seismicity rate change during the first 1.5 years after the Coalinga sequence (Figure 4d). The rate increase in the creeping section (km = –50 to 0) disappears after 1–2 years (Figure 4e). The seismicity rate cannot be reliably determined in areas rendered in gray. See color version of this figure at back of this issue.

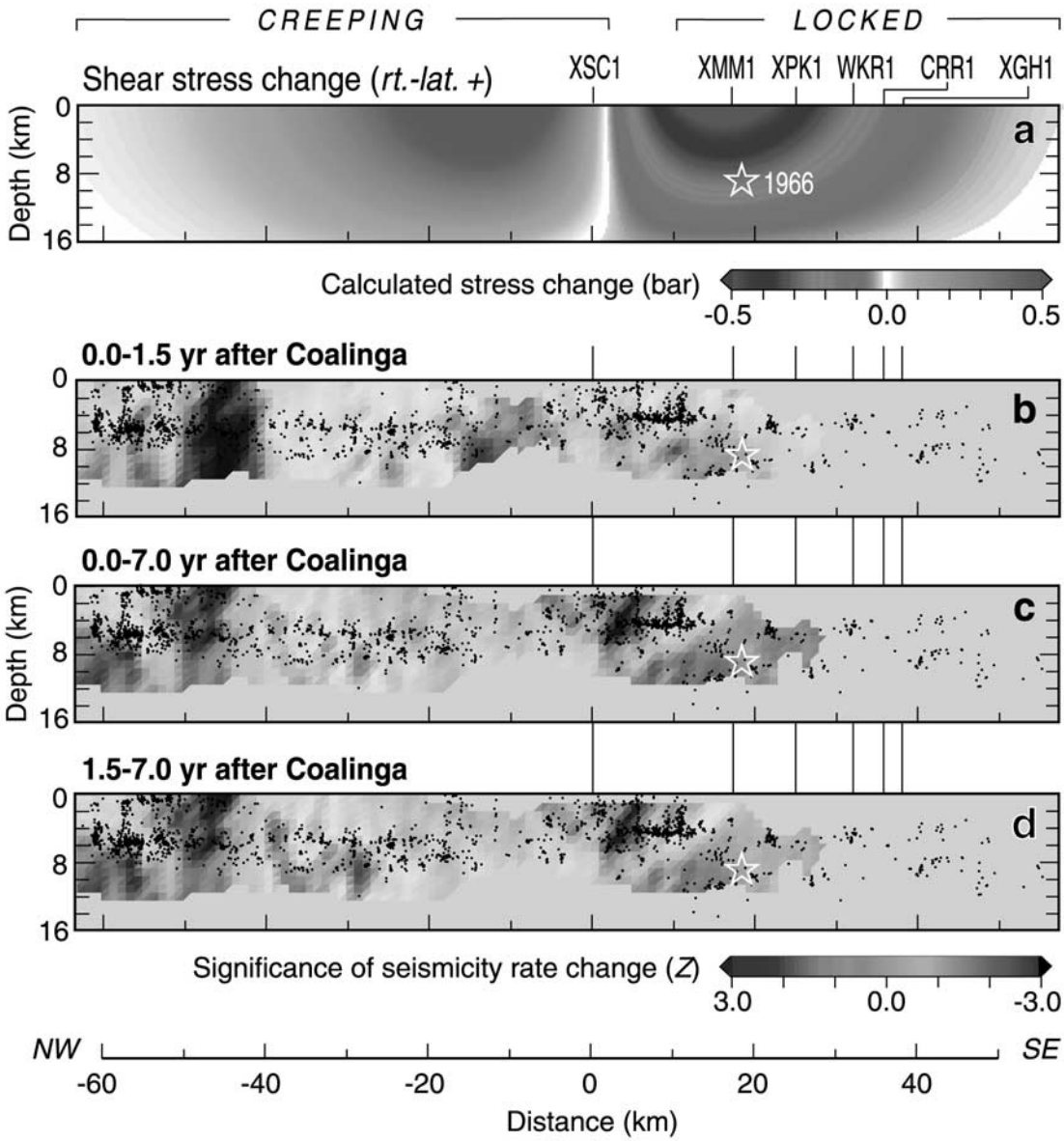

Figure 5. Calculation of the significance of the seismicity rate changes shown in Figure 4, using the Z statistic of *Habermann* [1983] and *Zuñiga and Wyss* [1995] (performed using Z map 5.0 of S. Wiemer, using a variable smoothing radius with r_{min} = 7.5 km, n = 100, and the "rubberband" function). Strong rate increases are evident in the creeping section, and somewhat weaker seismicity rate decreases are evident in the Parkfield hypocentral zone. Z values exceed ±3 in several key areas, although the paucity of earthquakes precludes calculation of the Z statistic southeast of the Parkfield hypocentral zone. See color version of this figure at back of this issue.

after the Coalinga earthquake [*Schulz et al.*, 1990], with the southern sites taking longest to recover (Figure 7a).

[10] The duration of retarded or reversed creep is correlated with the long-term creep rate: the faster the creep rate, the shorter the recovery time (Figure 7b). A linear correlation, for which R = 0.99, suggests that there would be no retardation where the creep rate equals the long-term San Andreas slip rate of ~23 mm/yr and that the recovery would last ~4–5 years south of Cholame, where the fault is fully locked. (A power law fit, in which the retardation period becomes infinite as the creep rate goes to zero, fits the data less well, with R = 0.84.) Coseismic offsets of 0.1–1.8 mm also accompanied the Coalinga shock [*Mavko et al.*, 1985]. In what follows, we model the observed creep series by calculating the amount a friction-less San Andreas would slip in order to shed the stress imposed by the 1983 shocks and subtract this induced slip from the long-term creep rate during the observed period of the creep retardation.

[11] To find the distribution of San Andreas slip needed to relieve the stress imposed by the Coalinga earthquakes, we treat the crust as an elastic half-space and represent the San Andreas fault as a planar grid of boundary elements [*Crouch and Starfield*, 1983] free to slip except where the fault is locked. We identify the locked region, where the fault slip rate is effectively zero, from the slip

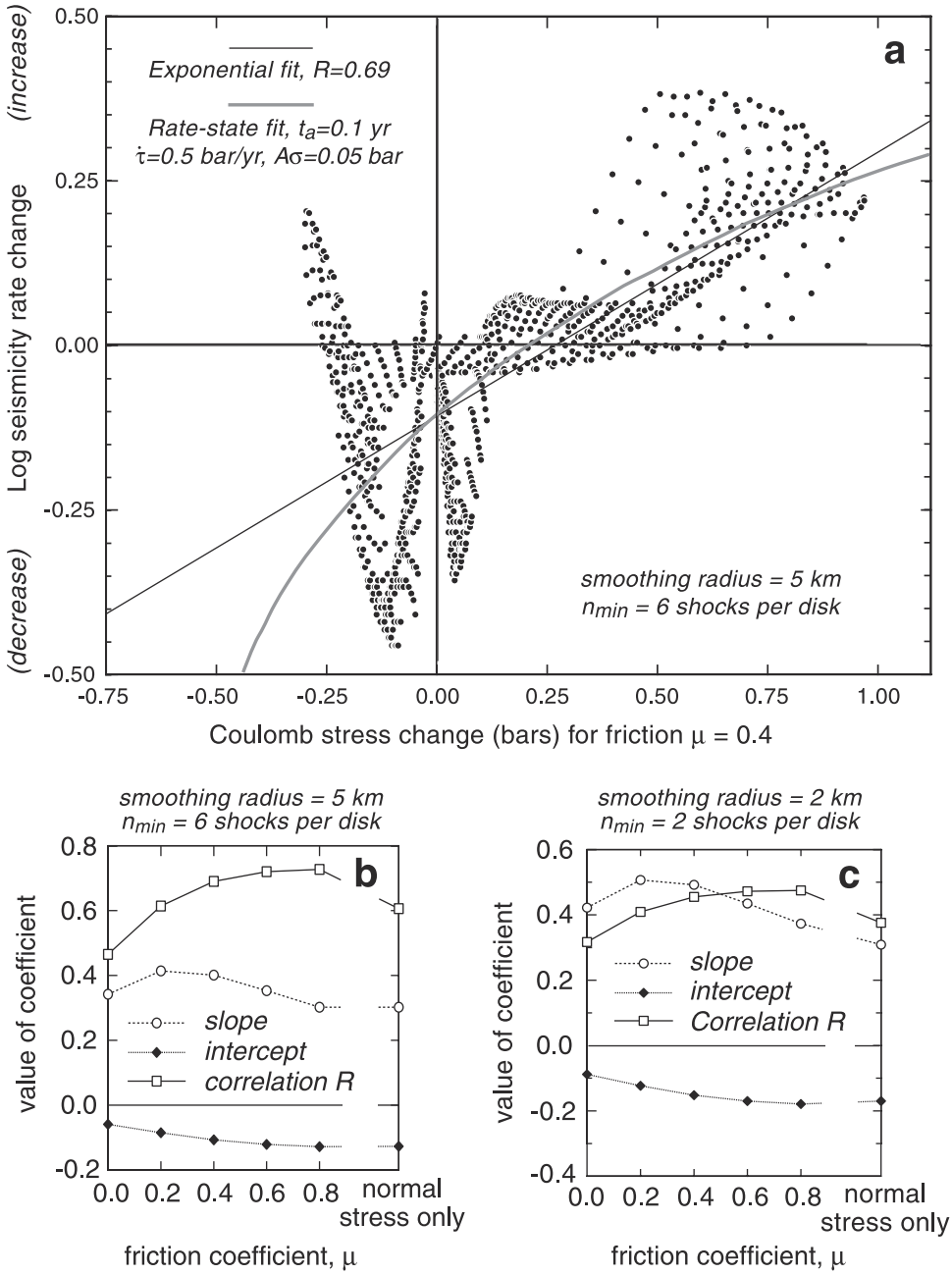

Figure 6. (a) Spatial regression of the calculated Coulomb stress change (with $\mu = 0.4$), from Figure 4c, on the observed seismicity rate change during the first 18 months after the Coalinga shock, from Figure 4d. Some 69% of the variance is accounted for by an exponential fit to the data (solid line). The positive Coulomb stress change data are also well fit by rate-state parameters appropriate for the creeping section (shaded curve). Dependence of the regression coefficients on friction, μ, for the data (b) as smoothed in Figure 4 and (c) when it is minimally smoothed.

rate inversion of GPS and long-term creep data by *Murray et al.* [2001], who discretized the fault into 2 × 3 km patches (Figure 8c). Such an elastic two-state model (the fault is either free to slip or fully locked) matches the decay of the long-term or secular creep rates toward the southeast (Figure 8a). Using the fault slipping/locked model of Figure 8c, we then find the slip needed to shed the stress imposed solely by the 1983 Coalinga-Nuñez shocks (Figure 8b). The effect of the 1983 shocks is to impose 6–25 mm of left-lateral slip, except at XSC1 where 9 mm of right-lateral slip is imposed. Finally, we subtract the imposed slip from the expected long-term creep over the observed period of creep retardation (Figure 7a). The result is that creep reverses where the ratio of the imposed slip over the retardation period is larger than the long-term creep rate. For example, at XMM1 the Coalinga shocks removed a calculated ~25 mm of San Andreas slip in 1 year; because this is greater

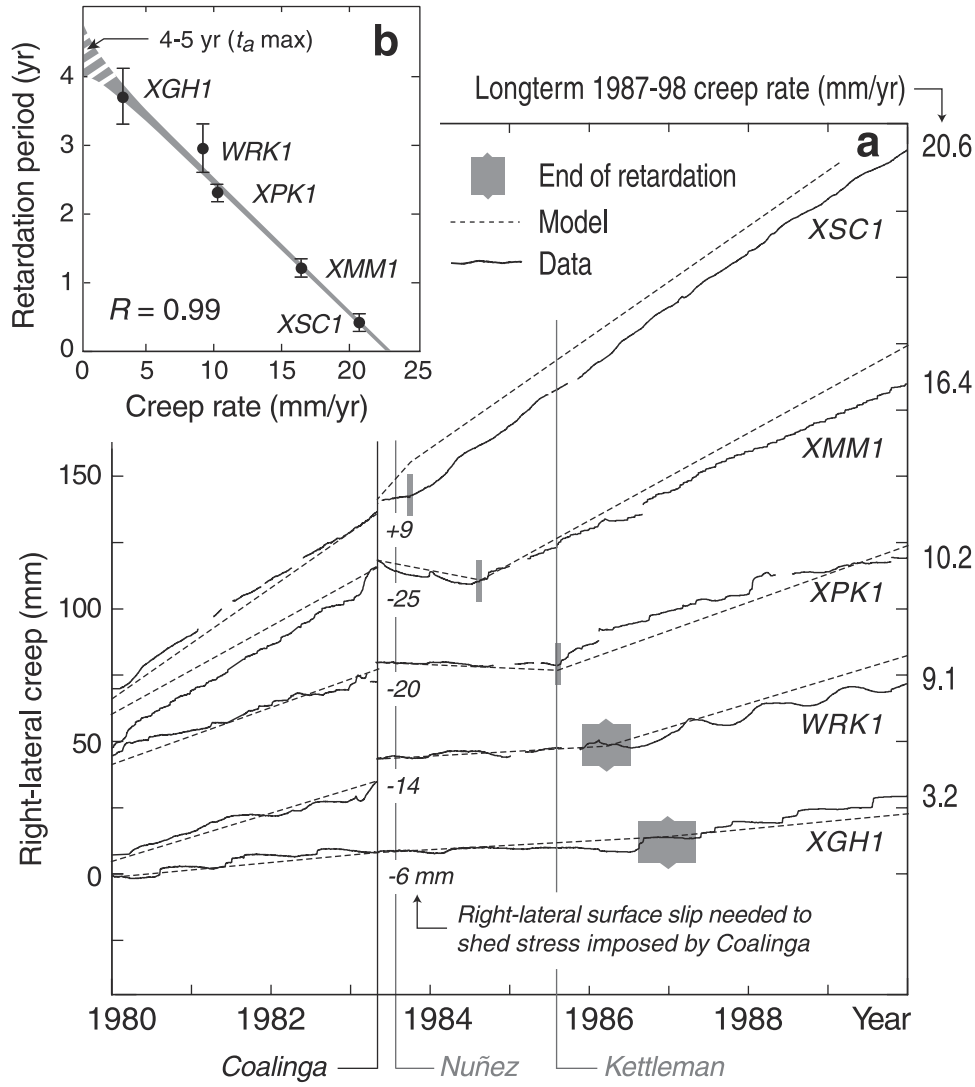

Figure 7. Response of creep meters to the Coalinga earthquake, with records displayed north to south (top to bottom). (a) Observed and modeled surface creep. Creep meter locations are shown in Figures 2a and 3. Rainfall is responsible for the rate increases in early 1983, but long-term creep rates and the creep retardation after Coalinga are judged reliable by *Roeloffs* [2001]. A 0.6-mm offset occurred on the day of the 4 August 1985 Kettleman Hills shock on XMM1, and the creep rate reversed on XPK1 5–6 days later. No other changes are evident at the time of the Kettleman Hills shock. The surface slip needed to shed the stress imposed by Coalinga, from Figure 11b, is also indicated, with right-lateral slip positive. Subtracting the slip imposed by Coalinga from the long-term slip rate over the period of observed creep retardation produces the modeled creep series (dashed). (b) The linear relationship between the creep retardation and the long-term creep rate suggests a maximum retardation in the locked Parkfield section of ~4.4 years; we equate this with the aftershock duration, t_a, for the locked section.

than the 16 mm/yr creep rate, the creep meter moved left laterally at 9 mm/yr for a year. The model matches most creep records; the largest departure is in the creeping section (XSC1), where accelerated creep is predicted but not observed.

6. Calculation of Earthquake Probability

[12] The time-dependent response of seismicity and creep to the stress imposed by the Coalinga-Nuñez sequence can be incorporated into an earthquake probability calculation [*Stein*, 1999]. In Coulomb failure theory a positive or negative stress change on the San Andreas fault causes an advance or delay to the time until failure is reached (Figure 9, top), resulting in a modest but permanent change in earthquake probability (Figure 9, thin solid lines in bottom panels). If this were a complete description of the process, then the Parkfield earthquake would be delayed by the stress change (−0.15 bar) divided by the stressing rate (~0.1 bar/yr), or 1–2 yr. However, such an approach fails to explain strong earthquake interactions on other faults. Examples include the order-of-magnitude decrease in $M \geq 6$ seismicity in the San

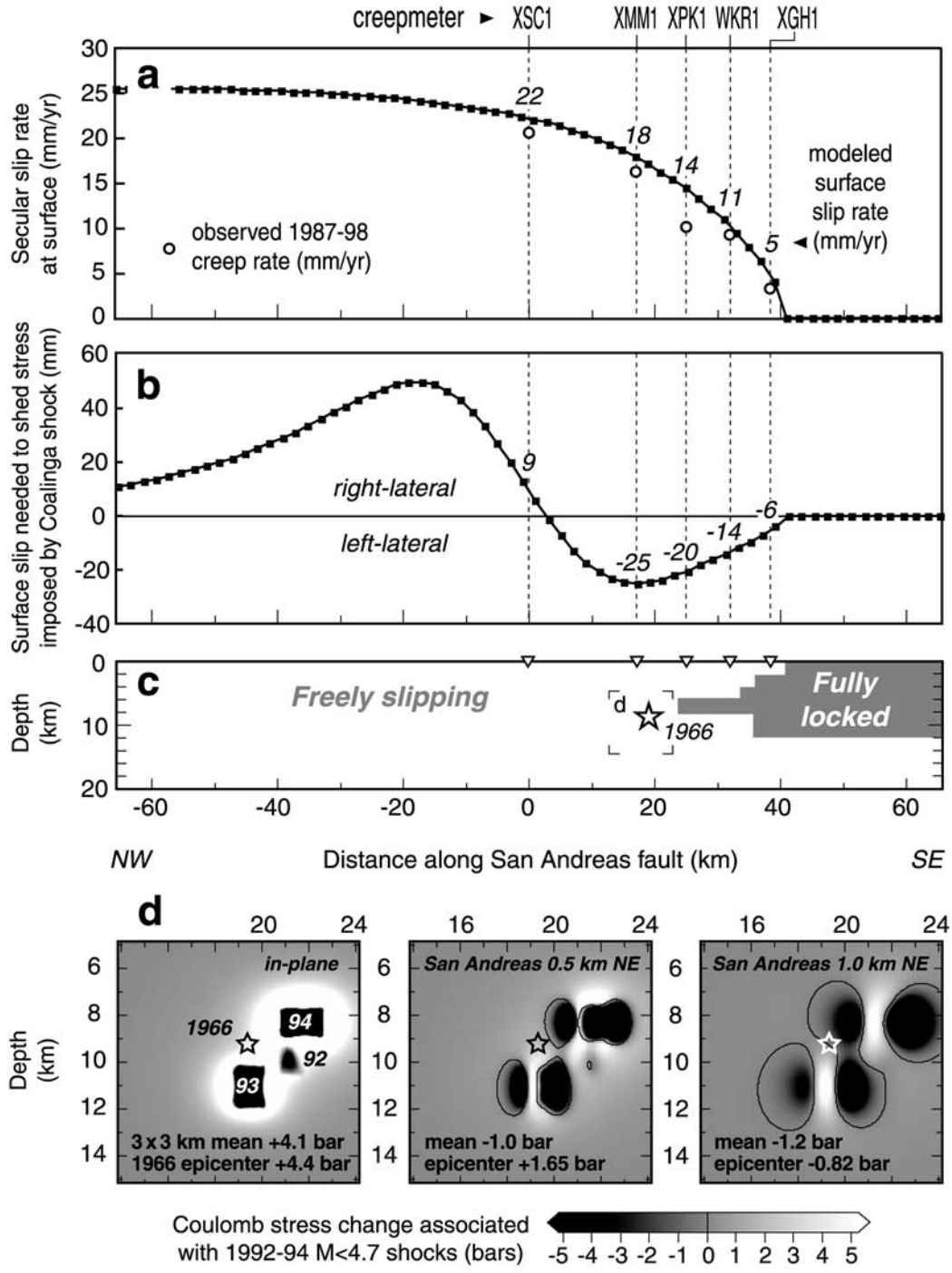

Figure 8. Calculated response of the San Andreas fault (a) to secular loading and (b) to stresses imposed by the 1983 Coalinga-Nuñez earthquakes. (c) The fault as represented by a grid of freely slipping boundary elements except where it is fully locked [*Murray et al.*, 2001]. The observed long-term creep rates (open circles in Figure 8a) are slightly lower than the model, appropriate if the creep meters do not span the full width of the fault zone. The calculated slip values in Figure 8b are reproduced in Figure 7a. (d) Stress changes in the 1966 hypocentral patch caused by the 20 October 1992 $M = 4.3$, 14 November 1993 $M = 4.6$, and 20 December 1994 $M = 4.7$ shocks [*Fletcher and Spudich*, 1998], which lie 0.5–1.0 km southwest of the main trace of the San Andreas fault near the 1966 hypocenter. The values at the ''1966 epicenter'' correspond to the star; the ''mean'' values are for the 3×3 km area centered on the star.

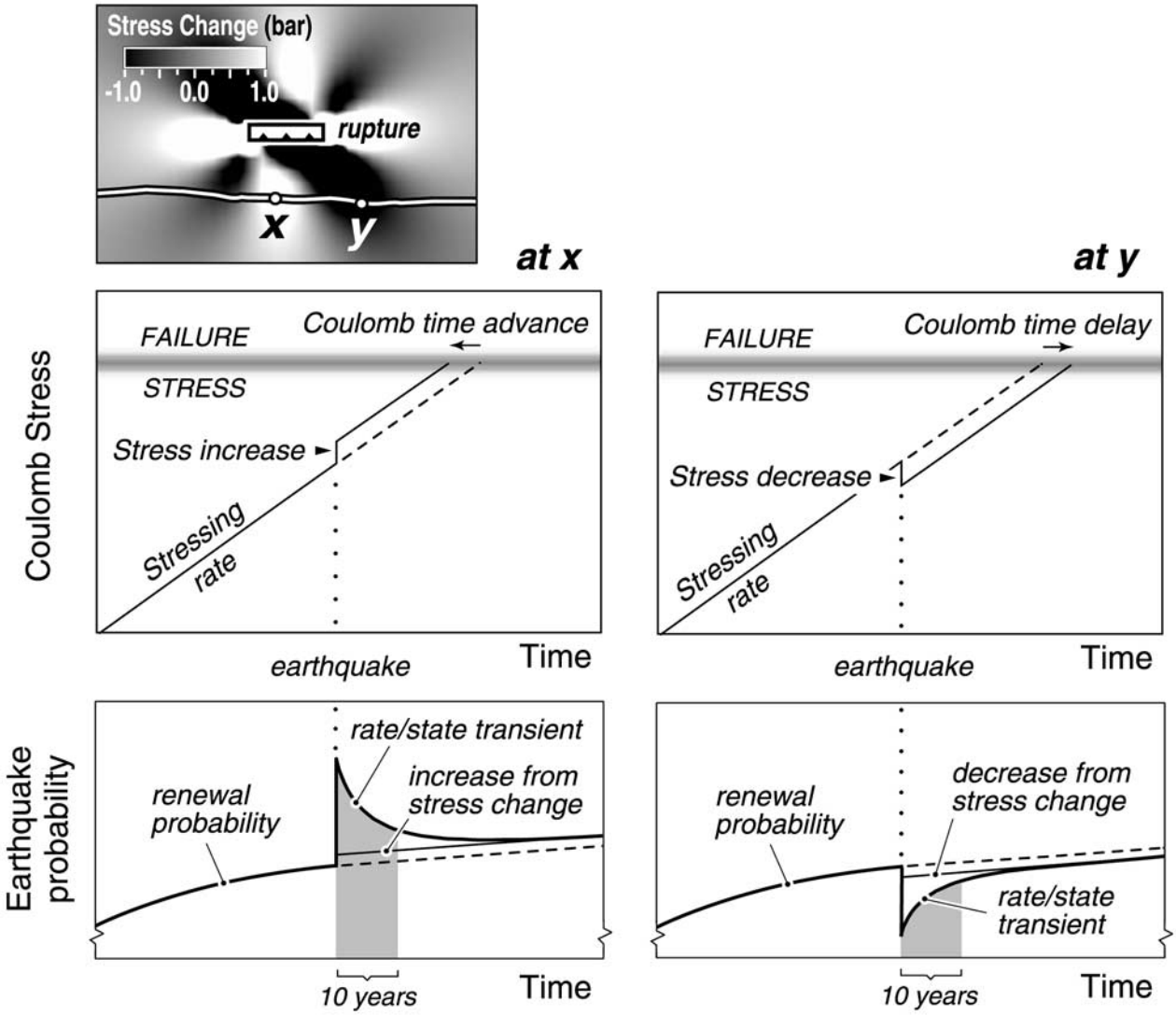

Figure 9. Schematic illustration of the effect of negative (at point *x*) and positive (at point *y*) stress changes on earthquake probability along a strike-slip fault, given an arbitrary off-fault earthquake source (rupture). The 10-year probability is the integral over the period in question. Rate-state effects of the shift to a time earlier or later in the earthquake cycle are neglected in this example. Bottom panels can be compared to the observed seismicity rate changes in both the creeping and Parkfield sections (Figure 11) and calculated probabilities for Parkfield (Figure 12).

Francisco Bay area during the 75 years after the great 1906 earthquake [*Bakun*, 1999; *Harris and Simpson*, 1998], and the 12 progressive $M \geq 6.7$ earthquakes along 1000 km of the North Anatolian fault during 1939–1999 [*Barka*, 1996; *Stein et al.*, 1997]. In such cases, the calculated static stress changes of several bars would at most advance or delay subsequent earthquakes by decades and could not explain seismicity rate changes persisting for 60–75 years.

[13] Our solution to this conundrum is to incorporate rate and state friction into the probability model, in which the transient effect of a stress decrease strongly amplifies the permanent decrease, because the fault slips at a lower rate, causing a lower rate of earthquake nucleation (Figure 9, bottom panels). The same phenomenon would apply to stress increases. Here seismicity is viewed as a sequence of nucleation events in which the state depends on the fault slip, slip rate, and elapsed time since the last event [*Dieterich*, 1994; *Dieterich and Kilgore*, 1996]. The seismicity rate equation is

$$R(t) = \frac{r}{\left[\exp\left(\frac{-\Delta \mathrm{CFF}}{A\sigma}\right) - 1\right]\exp\left(\frac{-t}{t_a}\right) + 1}, \qquad (2)$$

where R is the seismicity rate as a function of time, t, following a Coulomb stress change, ΔCFF, A is a constitutive parameter, σ is the total normal stress, t_a is the aftershock duration, and r is the seismicity rate before the stress perturbation, or the background seismicity rate.

[14] We seek the time-dependent seismicity rate $R(t)$ following a stress change ΔCFF on a fault, relative to the measured background rate, r. To evaluate (2), one

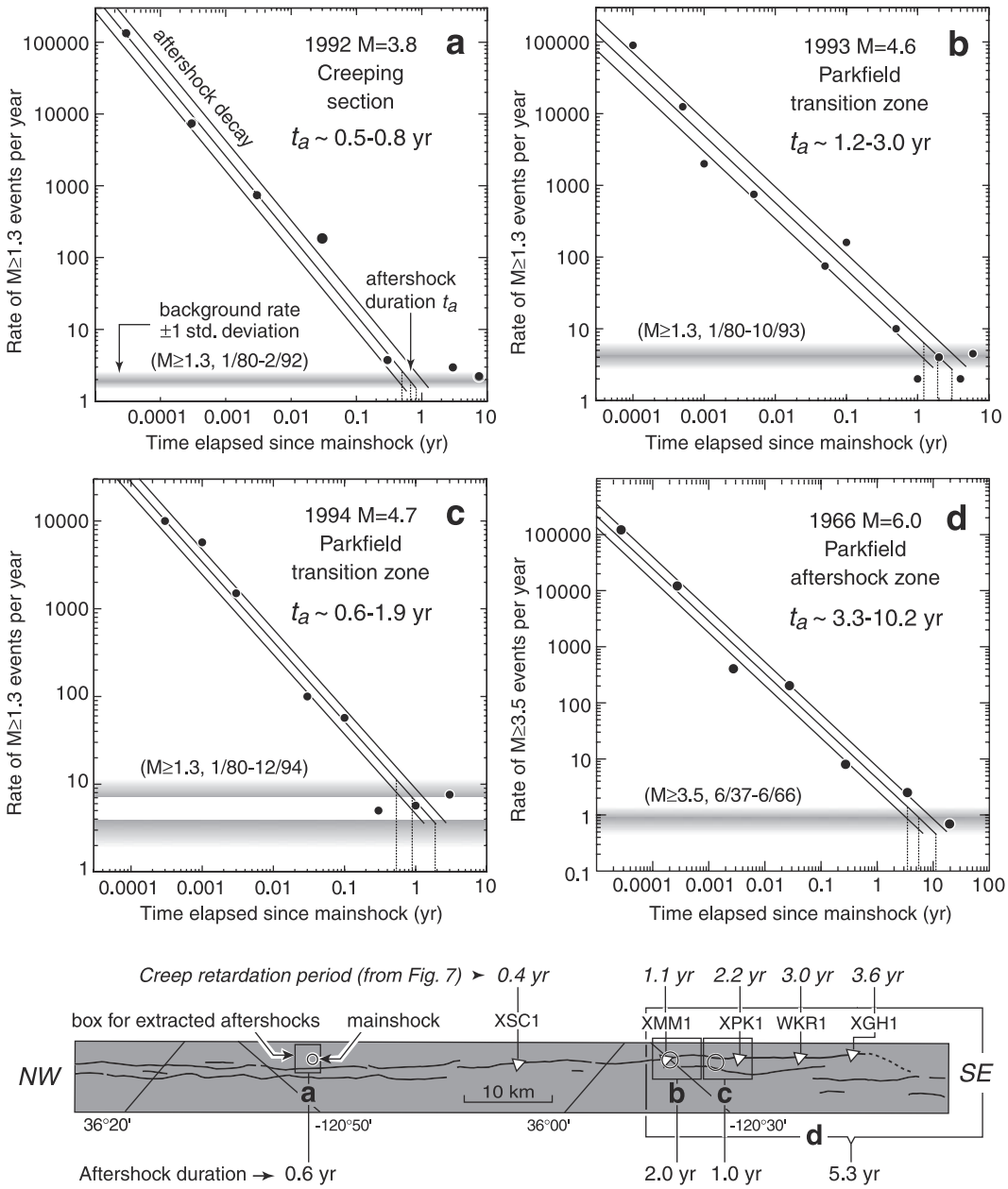

Figure 10. Estimated aftershock durations, t_a, along the San Andreas fault, with features labeled in Figure 10a and earthquake and creep meter locations shown in the bottom map. To permit the best possible calculation of the aftershock durations, the largest earthquakes along the creeping and Parkfield sections were selected at the four sites. Aftershocks were extracted from the NCSN catalog in the boxed regions; the background seismicity rate was estimated in the same boxes from 1980 until the time of the main shocks. For the 1966 earthquake the catalog of K. L. Meagher and C. S. Weaver (unpublished 1932–1969) was used, with the background rate estimated for 1937.5–1966.5. There is a general trend toward longer durations in the more fully locked part of the fault, consistent with the creep retardation periods in Figure 7.

calculates the stress change and estimates two of the following three properties: the fault stressing rate $\dot{\tau}$, the aftershock duration t_a, or $A\sigma$. To build the interaction into a renewal probability, one further assumes that with the passage of time from the last $M \sim 6$ shock in 1966, another such earthquake becomes more likely. For this, one must also assume a probability density function and estimate the elapsed time since the last earthquake, the interevent time, and the coefficient of variation for such events. Despite inevitable uncertainty in these assignments, the short repeat time, similar size, and long historical record for Parkfield earthquakes make estimates more reliable here than for most faults.

6.1. Aftershock Duration

[15] The transient decay is proportional to the aftershock duration, t_a, the time elapsed until the rate of seismicity returns to the rate that prevailed before the main shock

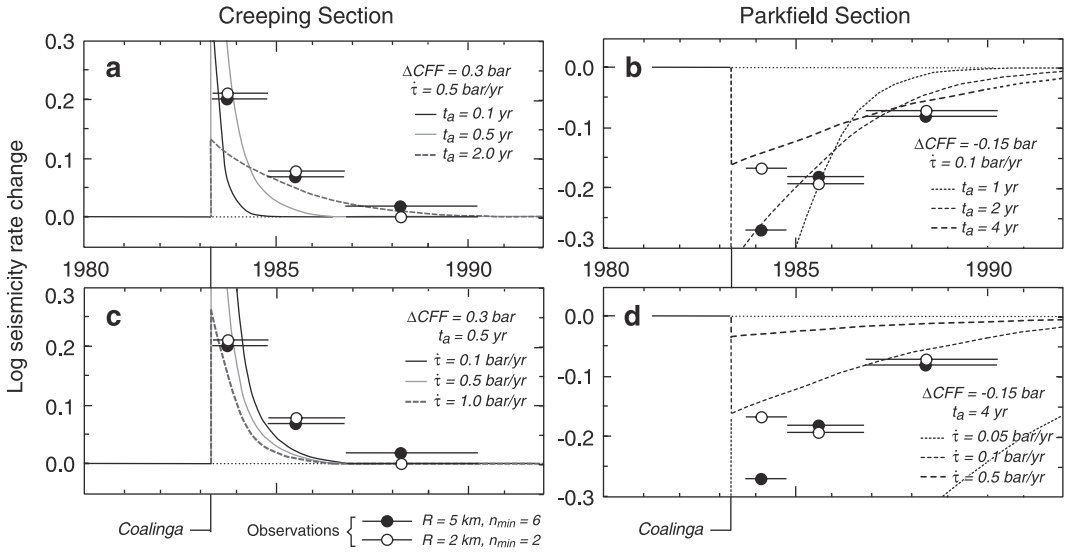

Figure 11. Observed and theoretical response of San Andreas seismicity to the 1983 Coalinga-Nuñez earthquakes. The observed seismicity rate changes are averages for the rectangles shown in mapview (Figure 2a) and in cross section (Figures 4d–4f). Seismicity rates have been shifted by a log rate change of −0.1, because of the negative seismicity rate bias discussed in the text, and indicated in Figure 6 as the y intercept. The mean Coulomb stress changes are from Figure 4c. (a) For t_a = 0.1 year, $A\sigma$ = 0.05 bar; for t_a = 0.5 year, $A\sigma$ = 0.25 bar; for t_a = 2.0 year, $A\sigma$ = 1.0 bar. (b) For t_a = 1 year, $A\sigma$ = 0.1 bar; for t_a = 2 years, $A\sigma$ = 0.2 bar; for t_a = 4 years, $A\sigma$ = 0.4 bar. (c) and (d) Varied stressing rate instead. The first interval covers 0.5–1.0 year after the Coalinga shock to avoid the time period of the swarm at km = 22 in Figure 4d. The seismicity rate change data are approximately fit by $t_a \sim 2$–4 years, in accord with creep (Figure 7b) and seismic data for the 1966 aftershock duration (Figure 10d).

occurred. In rate and state friction the aftershock duration t_a is related to $A\sigma$ through

$$t_a = A\sigma/\dot{\tau}, \tag{3}$$

where $\dot{\tau}$ is the fault stressing rate [*Dieterich*, 1994; *Dieterich and Kilgore*, 1996]; t_a is independent of main shock magnitude. We use the four largest main shocks on the San Andreas in the NCSN catalog to estimate aftershock duration as a function of position along the fault (Figures 10a–10d). There is an increase in aftershock duration toward the southeast, with durations growing from ∼0.6 year in the creeping section to ∼5 years in the locked region. Because we are limited by the small size of earthquakes in the creeping section, we cannot eliminate the possibility that the aftershock duration is a function of magnitude. However, the measured aftershock durations are comparable to the observed creep retardation periods (shown in the map in Figure 10), suggesting that the seismic and creep observations are manifestations of the same process: transient recovery to sudden stress changes. On the basis of the creep retardation periods of Figure 7 and the aftershock durations of Figure 10, we take t_a to be ∼0.5 year in the creeping section and ∼4.0 year in the locked Parkfield section.

[16] Although far from proven, these t_a assignments are consistent with another means to gauge the aftershock duration. The stressing rate, $\dot{\tau}$, can also be approximated by the main shock shear stress drop, $\Delta\tau$, divided by the interevent time, t_r, then from (3),

$$t_a = t_r(A\sigma/\Delta\tau). \tag{4}$$

In the Parkfield section the maximum observed earthquake magnitude $M_{\max}$ ∼6 and t_r ∼22 years. *Nadeau and Johnson* [1998] find that in the creeping section, $M_{\max}$ ∼4 and t_r ∼2.4 years. Thus, if earthquake stress drops and $A\sigma$ were constant in both locations, one would expect t_a to be roughly an order of magnitude larger in the locked section, consistent both with the observed creep retardation periods and aftershock durations.

6.2. Fault Stressing Rate

[17] We need to estimate the fault shear-stressing rate $\dot{\tau}$ at sites where earthquakes occur, as shown schematically in Figure 9 (top). Three approaches to estimation of $\dot{\tau}$ lead to different answers.

1. If the San Andreas were vertical, straight, and subject to the same plate boundary tractions (or alternatively, the same deep slip rate and locking depth) throughout the region of Figure 1, then its tectonic shear stressing rate should be uniform along strike. At a midcrustal depth of ∼8 km the shear stressing rate would be ∼0.1 bar/yr.

2. If one instead assumes that where the fault creeps stress is relieved, then the stressing rate would be near-zero in the creeping zone and much higher than 0.1 bar/yr at the north end of the locked zone, where dislocations would continuously pile up (Figure 8c).

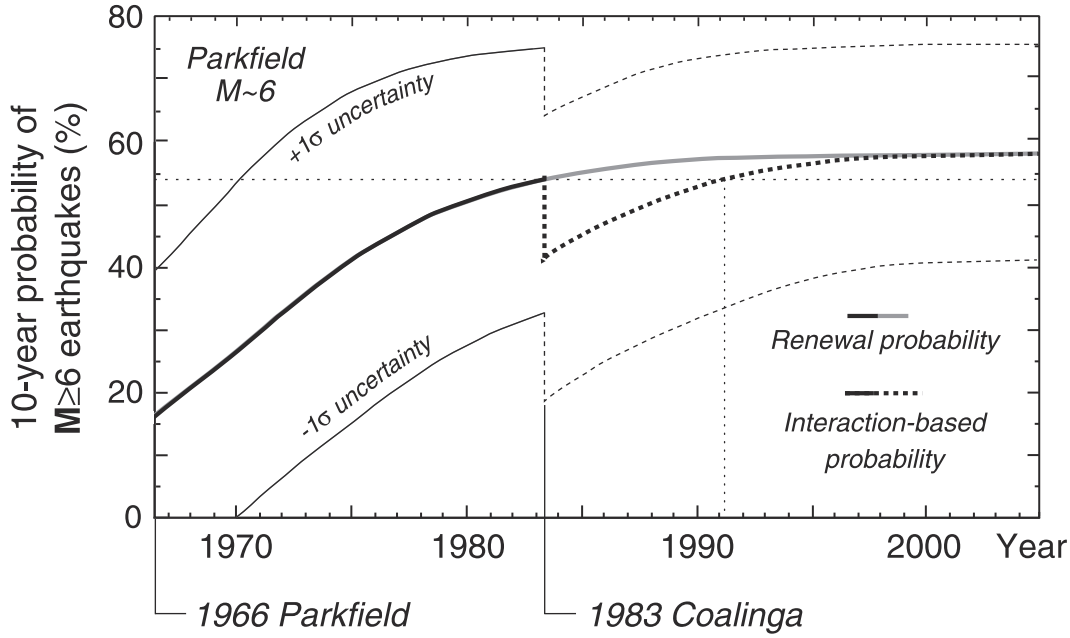

Figure 12. Ten-year probability of $M \geq 6$ earthquakes at Parkfield, calculated by Monte Carlo analysis following *Parsons et al.* [2000]. The 10-year probability drops from 54 ± 22% to 42 ± 23% as a result of the stress decrease imposed by the Coalinga earthquake and does not recover to pre-1983 values of probability until 1991. The 10-year probability of such an earthquake for 2001–2011 is calculated to be 58 ± 17%.

3. *Rubin et al.* [1999] and *Waldhauser et al.* [1999] find that seismicity in the creeping section is concentrated along isolated streaks, with the patches between streaks undergoing steady, aseismic creep. The stressing rate in the streaks would be higher than in the Parkfield locked patch, where the load is more uniformly distributed. (Streaks are not evident in Figures 4d–4g because pre-1984 data cannot be relocated by waveform cross correlation).

[18] Because we cannot confidently choose from these alternatives, we use the stressing rate that matches the observed seismicity rate as a function of time (Figure 11), and satisfies the creep retardation (Figure 7) and aftershock durations (Figure 10). This estimate is compatible only with the third alternative in the preceding paragraph and thus a rate appropriate for seismic streaks. The creeping section (Figure 11a) sustained a calculated mean 0.3-bar Coulomb stress increase, and t_a there is 0.5–1.0 year on the basis of Figure 10. The decay of the seismicity rate as a function of time is best fit by a stressing rate of 0.5 bar/yr, ~5 times higher than the average San Andreas stressing rate. This stressing rate is also compatible with the spatial regression of seismicity rate on stress change shown in Figure 6 (shading curve). Both the temporal and spatial seismicity rate data are fit by a high stressing rate in the creeping section. In the Parkfield section (Figure 11b) the mean calculated Coulomb stress change is −0.15 bars, and the data are satisfied by a stressing rate of 0.1 bar/yr for t_a = 2–4 years. Thus, given 1 degree of freedom (the stressing rate), we can satisfy the temporal decay of the seismicity rate following the Coalinga-Nuñez earthquakes.

6.3. Parkfield Probability

[19] The probability follows naturally from the seismicity rate change plot of Figure 11. We assume that the seismicity rate is altered not just for microearthquakes but for all magnitudes. Because $M \sim 6$ earthquakes are infrequent, there is only a chance that the rate change will result in a detectable change in the occurrence of a $M \sim 6$ event after 1983. We performed a Monte Carlo analysis of 1000 runs in which the tested values were drawn from a Gaussian distribution of the input parameters and plot the mean value and uncertainty as a function of time (Figure 12). The calculated stress change at the 5 × 5 km hypocentral site of the 1934 and 1966 earthquakes is −0.3 ± 0.1 bar (Figures 4b and 4c). The fault stressing rate (0.1 ± 0.025 bar/yr), aftershock duration (4 ± 1 years) are estimated from the preceding analysis of the creep and seismicity data. Calculations were made by running half the cases with lognormal and half with Brownian passage time [*Matthews et al.*, 2002] probability density functions, with mean interevent time of 22 years, and a coefficient of variation of 0.5 (given a range of 0.35 [*Savage*, 1993] to 0.70 [*Roeloffs and Langbein*, 1994]). The Brownian passage time is a renewal function with superposed Brownian noise; it has been used in the most recent working group probability analyses [*Working Group on California Earthquake Probabilities*, 1999]. The Monte Carlo analysis tests the full distribution of uncertainty, not simply the quoted 1σ error range.

[20] The calculated 10-year probability (Figure 12) in 1983 decreased from 54 ± 22% to 42 ± 23% and does not return to the pre-Coalinga probability until about 1991. October 1992 marked the beginning of a period of heightened seismic activity at Parkfield [*Michael and Jones*, 1998; *Fletcher and Guatteri*, 1999], including a M = 4.3 shock in 1992, a M = 4.6 shock in 1993, and a M = 4.7 shock in 1994). The occurrence of the renewed activity is consistent

with our probability calculation. Although the probability undergoes a fractional drop of 22% in 1983, it is not statistically significant. The rate-state effects of the stress change could be added to a Poisson model, as illustrated by *Toda et al.* [1998]. This would yield smaller nominal uncertainties because the coefficient of variation of the interevent time (0.5) would not enter into the calculations. However, we regard renewal as a better description of earthquake occurrence at Parkfield.

[21] The 1992–1994 earthquakes altered the stress at the site of the 1966 Parkfield hypocenter several kilometers away and thus changed the succeeding probability of future Parkfield earthquakes. We calculate the Coulomb stress changes associated with the 1992–1994 shocks on the hypocentral patch (for $\mu = 0.4$) using sources simplified from *Fletcher and Spudich* [1998], in which the slip is assumed to be pure right lateral on vertical coplanar faults (Figure 8d). Figure 8d (left) shows an increase in stress at the 1966 hypocenter by 4.4 bars if the sources are themselves coplanar with the 1966 hypocenter. If they were located 1 km to the northeast (Figure 8d, right), the stress would drop by 0.8 bar. The mean stress change in a 3×3 km Parkfield hypocentral patch is +4.1 bars if on the fault and −1.0 bar if the 1992–1994 shocks were just 0.5 km off the fault (Figure 8d). The main trace of the San Andreas lies 0.5–1.0 km northeast of the 1992–1994 shocks [*Fletcher and Guatteri*, 1999], and the location and depth of the 1966 hypocenter are uncertain by at least 1 km. Borehole tensor strain meters [*Gwyther et al.*, 1996] may provide additional evidence that the 1992–1994 shocks changed the conditions for future Parkfield earthquakes. The right-lateral shear strain rate increased starting in 1993 at two of three borehole instruments at Parkfield, although rainfall may influence or account for these signals, as discussed by *Gwyther et al.* [1996] and *Roeloffs* [2001]. Thus, while the effect of the 1992–1994 shocks on the 1966 hypocenter is likely large, the probability change depends on unknown features of the geometry of the patch and fault.

7. Comparison With Other Studies

[22] Several studies previously identified the seismicity rate decrease at Parkfield [*Miller*, 1996; *Poley et al.*, 1987; *Wyss et al.*, 1990], but the rate increase along the creeping section had escaped notice, perhaps because it is briefer and spatially restricted. *Wyss et al.* [1990] described a seismicity rate decrease in the Parkfield region that began 2 years after the Coalinga shock. We find that the rate decrease southeast of Parkfield instead began at the time of the Coalinga shock, but this was masked by the rate increase north of Parkfield, which did not end until ~18 months later. Thus the seismicity rate decrease that Wyss et al. ascribed to a process precursory to the next Parkfield earthquake we instead interpret as a response to the Coalinga shocks. *Wiemer and Wyss* [1997] found that the *a* and *b* values of the frequency-magnitude relation in the Parkfield hypocentral zone are anomalous with respect to the rest of the creeping and locked zones and attributed this to its role as a highly stressed asperity. They did not explore the change in these parameters after the Coalinga earthquake.

[23] *Simpson et al.* [1988] fit the creepmeter records to a model that is, like ours, driven by stressing from the deeper San Andreas fault and modulated by the stress change associated with the Coalinga earthquake. In their model the San Andreas stressing rate below 5 km is 0.75 bar/yr at XMM1 and 0.5 bar/yr at XGH1. They let the upper 5 km of the fault respond in a linear viscous manner to the stress changes, producing a left-lateral excursion at XMM1, and smaller left-lateral excursions on creep meters to the south, all of ~1-year duration. There is no tendency for creep retardation periods increasing toward the south, but the magnitudes of the creep changes resemble the observations. It is unclear, however, whether their modeled creep reversal occurred because they doubled the Coalinga coseismic slip to make the changes in the creep rates more apparent on their plots.

[24] Examining the 1983 coseismic offsets in the creep series, *Mavko et al.* [1985] found a rough match between the creepmeter offsets and calculated Coulomb stress changes for the Coalinga-Nuñez shocks, using $\mu = 0.6$. Analysis of the response of creepmeters to rainfall and earthquakes by *Roeloffs* [2001] indicates, however, that recentering of the instruments during shaking contaminates the coseismic displacements, whereas the creep rates before or after earthquakes suffer fewer such problems. Thus we offset the modeled creep series at the time of the Coalinga earthquake in Figure 7a.

[25] *Miller* [1996] proposed that unclamping of the Parkfield section of the San Andreas by the Coalinga earthquake, as shown in Figure 4a, decreased the pore fluid pressure in the fault zone, lowering the rate of fault weakening and inhibiting large earthquakes for an extended period. Unlike our explanation, in the work by *Miller* [1996] the shear stress changes (Figure 4b) have no role in changing the conditions for failure. Lacking any direct measurements of pore pressure or pore fluid flow, Miller supported his model by observations of seismicity rate, which he cites as rising from 1969 to 1983, dropping after the Coalinga event and remaining low through 1997. We instead regard the apparent increase in $M \geq 2.5$ seismicity rate from zero in 1969 as an artifact of inadequate reporting in the NCSN catalog. The K. L. Meagher and C. S. Weaver (unpublished 1932–1969) catalog, complete to $M \geq 3.5$ from 1934, shows a constant seismicity rate from 1940 to 1966. Further, the observed increase in seismicity rates during 1983–1985 in the creeping section (Figures 2c and 4d) is incompatible with Miller's model because this occurred where the unclamping was greatest. Miller does not explicitly consider the creep data, except to remark that changes in creep rates after 1983 are reconciled by the strengthening effect of homogenizing the shear stress along the fault. However, why creep rates reversed near Middle Mountain for up to a year and slowed or stopped farther south for 3–4 years is not explained. (Miller also predicted a Parkfield earthquake 34 years after the 1966 event (in 2000), which has not occurred.)

8. Conclusions

[26] We have sought to integrate the diverse observations at Parkfield in order to develop an understanding of the process by which stress contributes to or modulates the occurrence of earthquakes. We have argued that stress increases and decreases associated with nearby earthquakes influence subsequent seismicity. Seismicity and creep rates

are easily observed at Parkfield; they change at the time of the 1983 Coalinga-Nuñez shocks in a manner that resembles the calculated Coulomb stress change imparted by the 1983 shocks. The seismicity rate changes are robust, and the correlation of the changes with the Coulomb stress changes is statistically significant. The change in surface creep is also compatible with stress interaction. From creep and aftershock observations we infer that the San Andreas takes up to 10 times longer to recover from a stress perturbation where it is locked than where it creeps, consistent with rate-state friction.

[27] We argue that a probability model governed by rate and state friction and driven by steady stress buildup and stress transfer from nearby earthquakes can satisfy most of the Coalinga-Parkfield observations. We find the effect of the stress decrease on earthquake probability at Parkfield was larger and lasted longer than previously supposed and may have contributed to the absence of a Parkfield earthquake since 1983. Looking forward, we calculate that the probability of a $M \sim 6$ Parkfield shock today is higher than it was before 1983; during 2001–2011, we estimate a 58 ± 17% probability of a Parkfield earthquake. These prospective results are severely tempered, however, by uncertainty associated with the stress imparted by the 1992–1994 shocks near the site of the 1966 Parkfield nucleation.

[28] **Acknowledgments.** We are indebted to Jessica Murray, Tom Parsons, Paul Reasenberg, Evelyn Roeloffs, Paul Segall, Robert Simpson, Felix Waldhauser, Stefan Wiemer, and Max Wyss for their analytical tools, insight, and reviews. We gratefully acknowledge funding from PG&E.

References

Bakun, W. H., Seismic activity of the San Francisco Bay region, *Bull. Seismol. Soc. Am.*, *89*, 764–784, 1999.

Bakun, W. H., and T. V. McEvilly, Earthquakes near Parkfield, California: Comparing the 1934 and 1966 sequences, *Science*, *205*, 1375–1377, 1979.

Bakun, W. H., and T. V. McEvilly, Recurrence models and the Parkfield, California, earthquakes, *J. Geophys. Res.*, *89*, 3051–3058, 1984.

Barka, A. A., Slip distribution along the North Anatolian fault associated with large earthquakes of the period 1939 to 1967, *Bull. Seismol. Soc. Am.*, *86*, 1238–1254, 1996.

Crouch, S. L., and A. M. Starfield, *Boundary Element Methods in Solid Mechanics*, 322 pp., Allen Unwin, Concord, Mass., 1983.

Dieterich, J., A constitutive law for rate of earthquake production and its application to earthquake clustering, *J. Geophys. Res.*, *99*, 2601–2618, 1994.

Dieterich, J. H., and B. Kilgore, Implications of fault constitutive properties for earthquake prediction, *Proc. Natl. Acad. Sci. U.S.A.*, *93*, 3787–3794, 1996.

Eaton, J. P., The earthquake and its aftershocks from May 2 through September 30, 1983, in *The Coalinga, California, Earthquake of May 2, 1983*, edited by M. J. Rymer and W. L. Ellsworth, pp. 113–170, U.S. Geol. Surv., Washington, D. C., 1990.

Ekström, G., R. S. Stein, J. P. Eaton, and D. Eberhart-Phillips, Seismicity and geometry of a 110-km long blind thrust fault, 1, The 1985 Kettleman Hills, California, earthquake, *J. Geophys. Res.*, *97*, 4843–4864, 1992.

Fletcher, J. B., and M. Guatteri, Stress drop for three M ~ 4.3–4.7 (1992–1994) Parkfield, CA, earthquakes, *Geophys. Res. Lett.*, *26*, 2295–2298, 1999.

Fletcher, J. B., and P. Spudich, Rupture characteristics of the three M ~ 4.7 (1992–1994) Parkfield earthquakes, *J. Geophys. Res.*, *103*, 835–854, 1998.

Gwyther, R. L., M. T. Gladwin, M. Mee, and R. H. G. Hart, Anomalous shear strain at Parkfield during 1993–1994, *Geophys. Res. Lett.*, *23*, 2425–2428, 1996.

Habermann, R. E., Teleseismic detection in the Aleutian Island arc, *J. Geophys. Res.*, *88*, 5056–5064, 1983.

Harris, R. A., and R. W. Simpson, Suppresion of large earthquakes by stress shadows: A comparison of Coulomb and rate-and-state, *J. Geophys. Res.*, *103*, 24,439–24,451, 1998.

Matthews, M. V., and P. A. Reasenberg, Statistical methods for investigating quiescence and other temporal seismicity patterns, *Pure Appl. Geophys.*, *126*, 357–372, 1988.

Matthews, M. V., W. L. Ellsworth, and P. A. Reasenberg, A Brownian model for recurrent earthquakes, *Bull. Seismol. Soc. Am.*, in press, 2002.

Mavko, G. M., S. Schulz, and B. D. Brown, Effects of the 1983 Coalinga, California, earthquake on creep along the San Andreas fault, *Bull. Seismol. Soc. Am.*, *75*, 475–489, 1985.

Michael, A. J., and L. M. Jones, Seismicity alert probabilities at Parkfield, California, revisited, *Bull. Seismol. Soc. Am.*, *88*, 117–130, 1998.

Miller, S. A., Fluid-mediated influence of adjacent thrusting on the seismic cycle at Parkfield, *Nature*, *382*, 799–802, 1996.

Murray, J., P. Segall, P. Cervelli, W. Prescott, and J. Svarc, Inversion of GPS data for spatially variable slip-rate on the San Andreas fault at Parkfield, CA, *Geophys. Res. Lett.*, *28*, 359–362, 2001.

Nadeau, R. M., and L. R. Johnson, Seismological studies at Parkfield, IV, Moment release and estimates of source parameters for small repeating earthquakes, *Bull. Seismol. Soc. Am.*, *88*, 790–814, 1998.

Parsons, T., R. S. Stein, R. W. Simpson, and P. A. Reasenberg, Stress sensitivity of fault seismicity: A comparison between limited-offset oblique and major strike-slip faults, *J. Geophys. Res.*, *104*, 20,183–20,202, 1999.

Parsons, T., S. Toda, R. S. Stein, A. Barka, and J. H. Dieterich, Heightened odds of large earthquakes near Istanbul: An interaction-based probability calculation, *Science*, *288*, 661–665, 2000.

Poley, C. M., A. G. Lindh, W. H. Bakun, and S. S. Schulz, Temporal changes in microseismicity and creep near Parkfield, California, *Nature*, *327*, 134–137, 1987.

Reasenberg, P. A., and R. W. Simpson, Response of regional seismicity to the static stress change produced by the Loma Prieta earthquake, *Science*, *255*, 1687–1690, 1992.

Roeloffs, E. A., Creep rate changes at Parkfield, California 1966–1999: Seasonal, precipitation-induced and tectonic, *J. Geophys. Res.*, *106*, 16,525–16,547, 2001.

Roeloffs, E., and J. Langbein, The earthquake prediction experiment at Parkfield, California, *Rev. Geophys.*, *32*, 315–336, 1994.

Rubin, A. M., D. Gillard, and J.-L. Got, Streaks of microearthquakes along creeping faults, *Nature*, *400*, 635–641, 1999.

Rymer, M. J., K. J. Kendrick, J. J. Lienkaemper, and M. M. Clark, Surface rupture on the Nuñez fault after June 11, 1983, in *The Coalinga, California, Earthquake of May 2, 1983*, edited by M. J. Rymer and W. L. Ellsworth, pp. 299–318, U.S. Geol. Surv., Washington, D. C., 1990.

Savage, J. C., The Parkfield prediction fallacy, *Bull. Seismol. Soc. Am.*, *83*, 1–6, 1993.

Schulz, S. S., G. Mavko, and B. D. Brown, Response of creepmeters on the San Andreas fault near Parkfield to the earthquake, in *The Coalinga, California, Earthquake if May 2, 1983*, edited by M. J. Rymer and W. L. Ellsworth, pp. 409–417, U.S. Geol. Surv., Washington, D. C., 1990.

Segall, P., and Y. Du, How similar were the 1934 and 1966 Parkfield earthquakes?, *J. Geophys. Res.*, *98*, 4527–4538, 1993.

Simpson, R. W., S. S. Schulz, L. D. Dietz, and R. O. Burford, The response of creeping parts of the San Andreas fault to earthquakes on nearby faults: Two examples, *Pure Appl. Geophys.*, *126*, 665–684, 1988.

Stein, R. S., The role of stress transfer in earthquake occurrence, *Nature*, *402*, 605–609, 1999.

Stein, R. S., and G. E. Ekström, Seismicity and geometry of a 110-km long blind thrust fault, 2, Synthesis of the 1982–85 California earthquake sequence, *J. Geophys. Res.*, *97*, 4865–4883, 1992.

Stein, R. S., A. A. Barka, and J. H. Dieterich, Progressive failure on the North Anatolian fault since 1939 by earthquake stress triggering, *Geophys. J. Int.*, *128*, 594–604, 1997.

Toda, S., R. S. Stein, P. A. Reasenberg, and J. H. Dieterich, Stress transferred by the M_w = 6.5 Kobe, Japan, shock: Effect on aftershocks and future earthquake probabilities, *J. Geophys. Res.*, *103*, 24,543–24,565, 1998.

Waldhauser, F., and W. L. Ellsworth, A double-difference earthquake location algorithm: Method and application to the northern Hayward fault, California, *Bull. Seismol. Soc. Am.*, *90*, 1353–1368, 2000.

Waldhauser, F., W. L. Ellsworth, and A. Cole, Slip-parallel seismic lineations on the northern Hayward fault, California, *Geophys. Res. Lett.*, *26*, 3525–3528, 1999.

Wiemer, S., and M. Wyss, Mapping the frequency-magnitude distribution in asperities: An improved technique to calculate recurrence times?, *J. Geophys. Res.*, *102*, 15,115–15,128, 1997.

Wiemer, S., and M. Wyss, Minimum magnitude of completeness in earthquake catalogs: Examples form Alaska, the western United States, and Japan, *Bull. Seismol. Soc. Am.*, *90*, 859–869, 2000.

Working Group on California Earthquake Probabilities, Earthquake probabilities in the San Francisco Bay region: 2000 to 2030—A summary of findings, *U.S. Geol. Surv. Open File Rep.*, 99–517, 1999.

Wyss, M., and S. Wiemer, Change in the probability for earthquakes in southern California due to the Landers magnitude 7.3 earthquake, *Science*, *290*, 1334–1338, 2000.

Wyss, M., P. Bodin, and R. E. Habermann, Seismic quiescence at Parkfield: An independent indication of an imminent earthquake, *Nature*, *345*, 426–431, 1990.

Zuñiga, R., and M. Wyss, Inadvertant changes in magnitude reported in earthquake catalogs: Their evaluation through b-value estimates, *Bull. Seismol. Soc. Am.*, *86*, 1858–1866, 1995.

R. S. Stein, U.S. Geological Survey, 345 Middlefield Road, MS 977, Menlo Park, CA 94025, USA. (rstein@usgs.gov)

S. Toda, Active Fault Research Center, Geological Survey of Japan, AIST, Higashi 1-1, Tsukuba, Japan 305-8567. (s-toda@aist.go.jp)

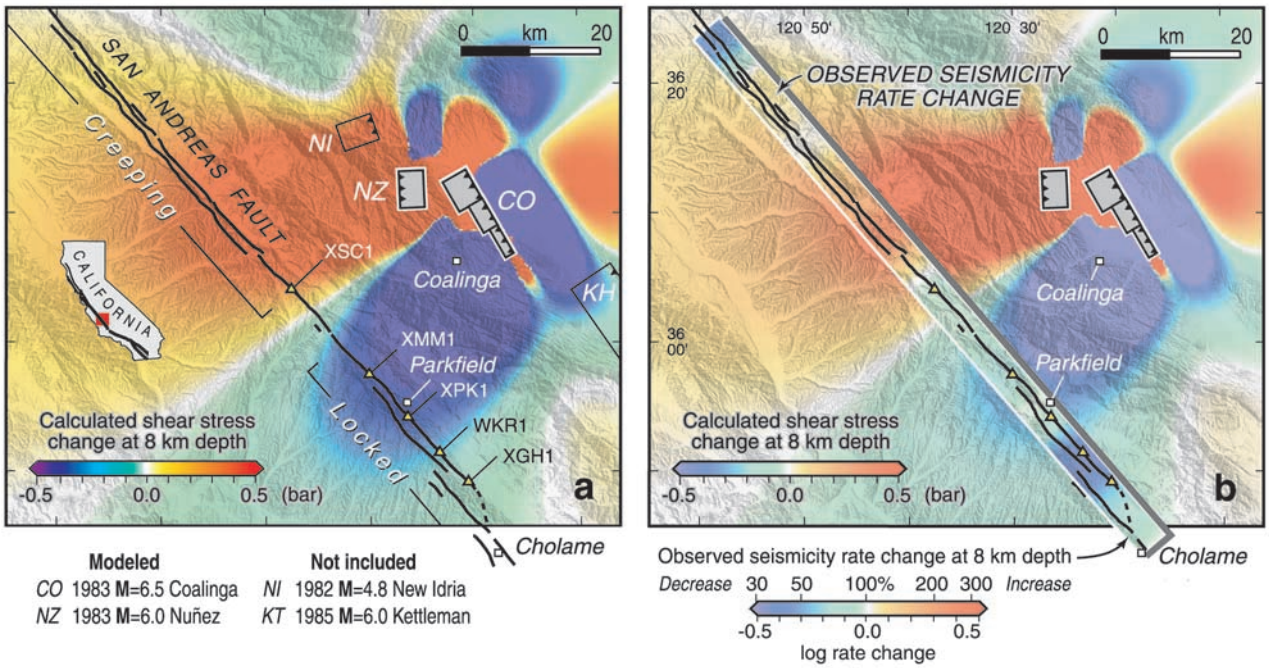

Figure 1. (a) Shear stress transferred by the 2 May 1983 $M = 6.5$ Coalinga (CO) and 11 June to 22 July $M = 6.0$ Nuñez (NZ) earthquakes on vertical right-lateral planes parallel to the San Andreas fault at 8 km depth. Source parameters for CO are from *Stein and Ekström* [1992] for the coseismic period: 150° strike, 15°W dip, 4.7 m reverse slip, 10 km upper depth, and 1.5–4.0 km width; for NZ they are based on work by *Eaton* [1990] and *Rymer et al.* [1990]: 178° strike, 65°E dip, 0.22 m right-lateral and 0.65 m reverse slip, 5.4 km length, and 2 km upper and 8.3 km width. Excluded because of their negligible impact on the stress are the 25 October 1982 $M = 4.8$ New Idria (NI) shock and the 4 August 1985 $M = 6.0$ Kettleman Hills (KH) shock [*Ekström et al.*, 1992]. (b) The observed seismicity rate change is superimposed along the San Andreas fault, also at 8 km depth. Relocated $M = 1.3$ seismicity is from the NCSN in a 10-km-wide box with endpoints at 36.50°/−121.08° 35.65°/−120.20°.

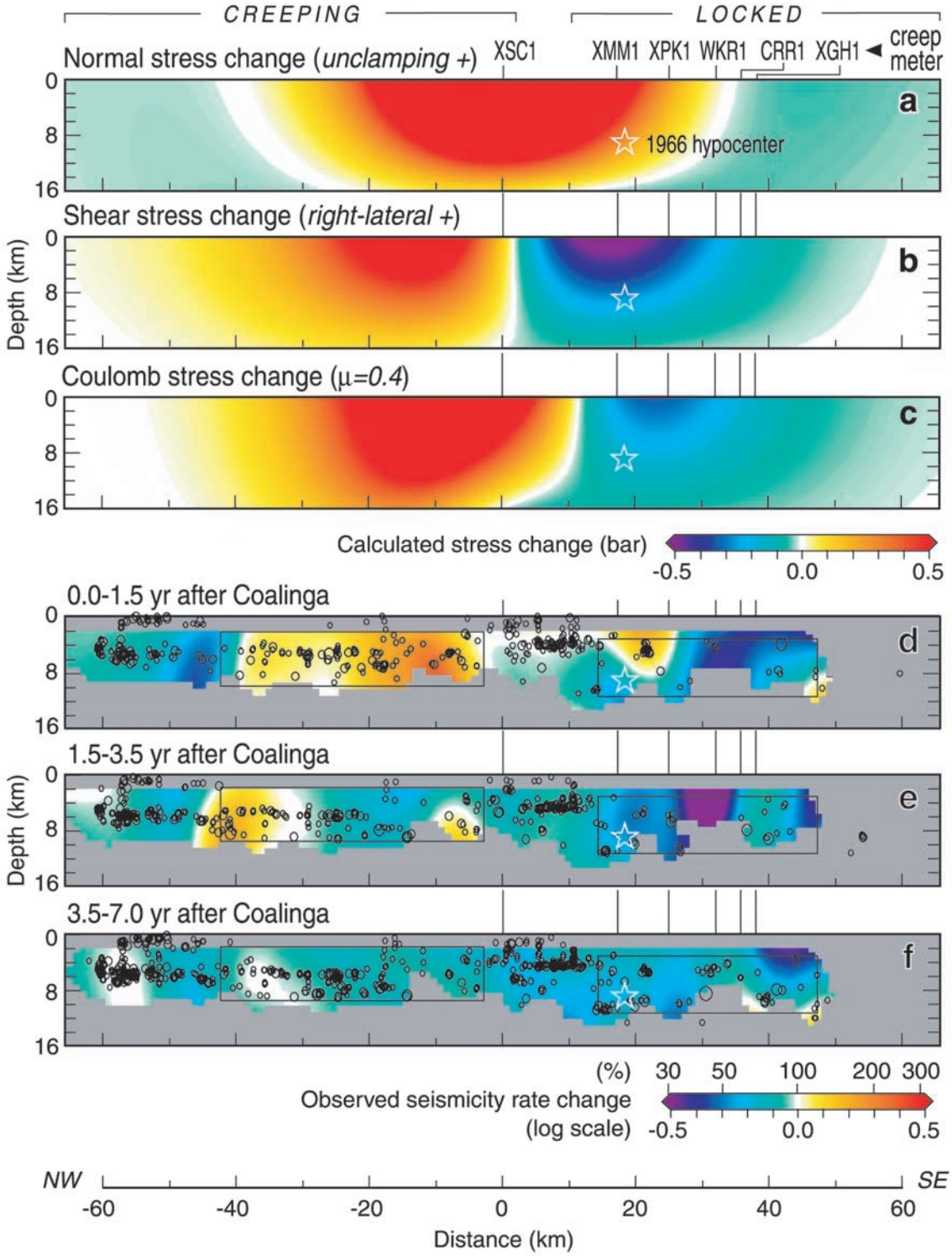

Figure 4. (a) Calculated normal, (b) shear, and (c) Coulomb stress change and (d–f) observed seismicity rate change within 5 km of the San Andreas fault associated with the 1983 Coalinga-Nuñez shocks, with earthquakes during the indicated post-Coalinga period superimposed in black. The seismicity rate change for the post-Coalinga 1.5-year period 2 May 1983 to 1 November 1984 (Figure 4d) and the 5.5-year period 2 November 1984 to 1 May 1990 (Figure 4e) are calculated relative to the 3-year pre-Coalinga period 2 May 1980 to 1 May 1983. The stress changes are similar to those of *Simpson et al.* [1988]. Note the association between the calculated shear stress change (Figure 4b) and the observed seismicity rate change during the first 1.5 years after the Coalinga sequence (Figure 4d). The rate increase in the creeping section (km = –50 to 0) disappears after 1–2 years (Figure 4e). The seismicity rate cannot be reliably determined in areas rendered in gray.

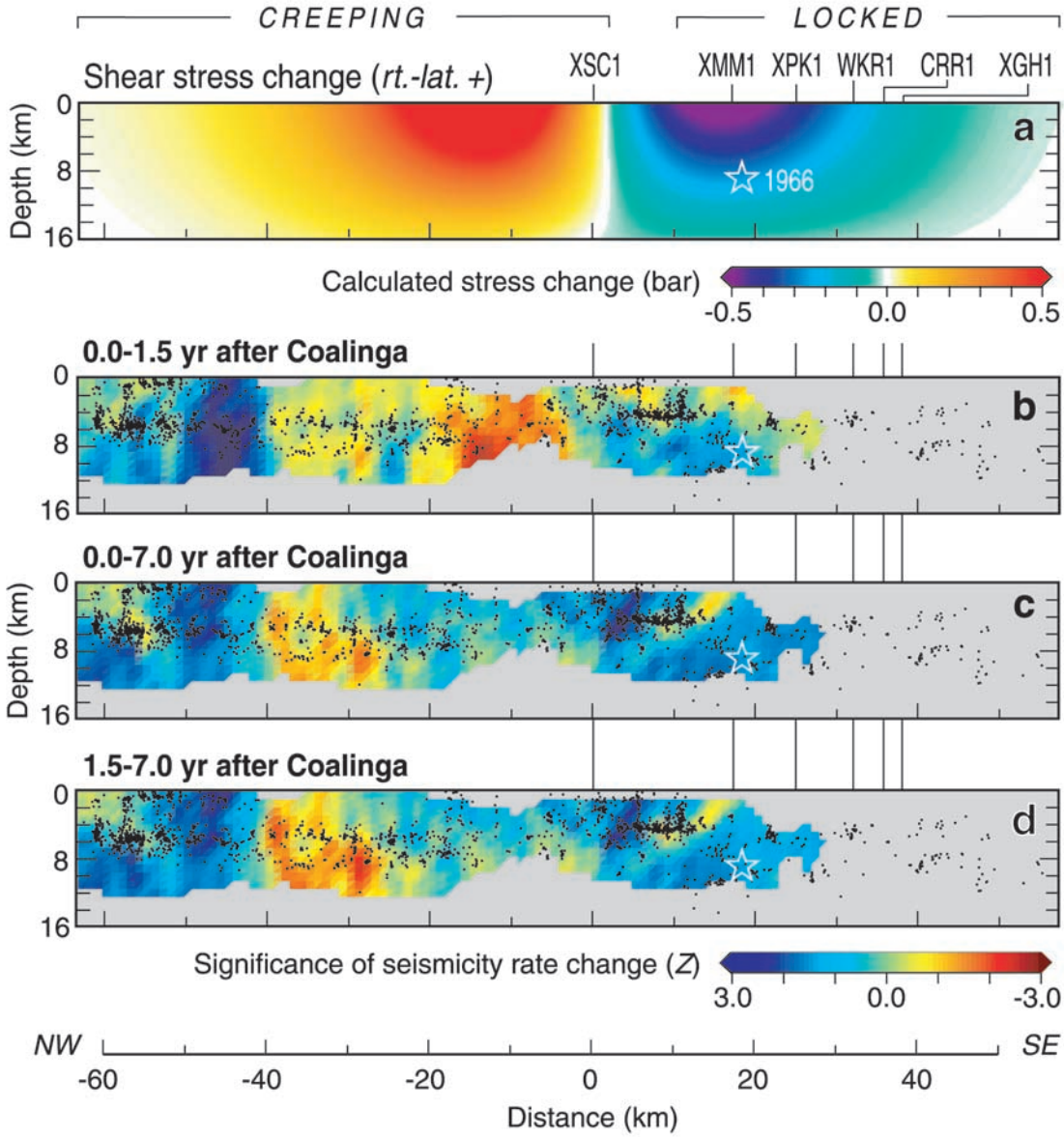

Figure 5. Calculation of the significance of the seismicity rate changes shown in Figure 4, using the *Z* statistic of *Habermann* [1983] and *Zuñiga and Wyss* [1995] (performed using Z map 5.0 of S. Wiemer, using a variable smoothing radius with r_{min} = 7.5 km, n = 100, and the "rubberband" function). Strong rate increases are evident in the creeping section, and somewhat weaker seismicity rate decreases are evident in the Parkfield hypocentral zone. *Z* values exceed ±3 in several key areas, although the paucity of earthquakes precludes calculation of the *Z* statistic southeast of the Parkfield hypocentral zone.